Third Sound Analysis of Superfluid ^{4}He Films Adsorbed on Multiwall Carbon Nanotubes

Lara Mitchell
Department of Physics and Astronomy, University of California, Los Angeles, California 90095

Abstract

Third sound is known to depend on the chemistry and geometry of the substrate on which a superfluid film is adsorbed. We have studied third sound in films adsorbed on multiwall carbon nanotubes to determine the effects of the cylindrical nanotube geometry. The Van der Waals potential for a single nanotube and the theoretical propagation velocity on the outer surface of a nanotube are presented. The nanotube geometry is found to lower both the potential and third sound velocity, and strongly limit the film thickness. Preliminary third sound measurements are presented for films on multiwall nanotubes 10 – 20 nm in diameter at 1.3 K. In addition to possible signs of capillary condensation, a novel re-entrant behavior of the superfluidity is observed: as the film thickness is increased near 3 atomic layers a superfluid signal is observed, but it disappears with the addition of further helium, and then reappears when the film thickness is further increased. This unusual behavior may be due to quasi-solidification of the helium when the third layer is just completed. The use of nanotubes is motivated by the possibility of a two-dimensional to one-dimensional crossover at low enough temperatures.

Introduction

Extensive theoretical and experimental work has been done on the superfluid phase transition using superfluid ^{4}He thin films. The two-dimensional transition on a flat substrate is described by the Kosterlitz-Thouless vortex model, which predicts an abrupt drop in superfluid density to zero at a critical temperature dependent on film thickness. Currents generated by thermally excited vortex-antivortex pairs reduce an applied current in the fluid, lowering the superfluid density. Films adsorbed on porous substrates exhibit a broadened Kosterlitz-Thouless transition curve and a decrease in third sound attenuation [1]. Such features have been observed on porous materials including Vycor glass and packed alumina powder [2,3]. These characteristics are interpreted as the crossover from a two-dimensional to three-dimensional phase transition which occurs as the vortex separation exceeds the pore length [1]. The three-dimensional transition is caused by thermally excited three-dimensional vortex rings which increase in size with increasing temperature [4]. The possibility of a two-dimensional to one-dimensional crossover was suggested by Machta and Guyer in 1989 in their analysis of superfluid adsorption on a cylindrical surface [5]. Experimental studies using MCM-41, which consists of cylindrical pores, have also suggested a 1 dimensional crossover, though the results are not conclusive [6].

With the present-day availability of carbon nanotubes, first discovered in the 1990's, it is possible to experimentally investigate superfluid behavior on a substrate with cylindrical geometry. Nanotubes are composed of sheets of graphite rolled into hollow tubes of variable length, thickness, and diameter [7]. Third sound signals have already been observed on singlewall nanotube bundles with 5 nm diameter [8]. In this work we focus on the

adsorption properties of multiwall nanotubes. Calculations indicate that the surface tension force resulting from the curvature of a nanotube plays an important role in determining the thickness of the film that can form on the nanotube surface. The Van der Waals potential of the nanotubes and the third sound velocity of the film are also affected by the nanotube geometry. Preliminary third sound measurements have been carried out at 1.3 K using multiwall carbon nanotubes with an average diameter of 15 nm. We have observed a re-entrant behavior in the superfluidity following the onset point just above 3 atomic layers.

Theory

Here we present a theoretical analysis of superfluid film adsorption on a single nanotube and compare the results to the well-studied results for film adsorption on a flat substrate. The most important factor in our analysis is the cylindrical geometry of a nanotube.

Third sound propagation depends on an attractive, restoring Van der Waals force between the helium and substrate atoms [9]. For a flat substrate, the Van der Waals potential energy is $U(z) = -\alpha/z^3$, where α is a constant specific to the substrate material and z is the distance to the substrate. The potential between a spherical particle and infinite cylinder in a non-retarded interaction, as calculated by Kirsch [10], is

$$U_c(y) = -\pi^{3/2}\alpha n_c \frac{\Gamma\left(\frac{m-1}{2}\right)}{\Gamma\left(\frac{m}{2}\right)} \frac{R^2}{y^{m-1}} F\left(\frac{m-1}{2}, \frac{m-1}{2}; 2; \frac{R^2}{y^2}\right)\Bigg|_{m=6} \quad (1)$$

where n_c is the concentration of particles, R is the cylinder radius, y is the closest distance between the particle and cylinder axis, $\Gamma(x)$ is the Gamma Function, and F(a,b;c;x) is the Gauss hypergeometric function. Applying this model to a spherical helium atom and a long cylindrical nanotube with y = R + z, the potential becomes

$$U_c(z) = -\frac{3\pi^2\alpha n_c}{8} \frac{R^2}{(R+z)^5} F\left(\frac{5}{2}, \frac{5}{2}; 2; \frac{R^2}{(R+z)^2}\right) \quad (2)$$

As $R \to \infty$, the potential should reduce to that between a helium atom and flat substrate. The normalized potential $\hat{U}(z)$ and the first two terms of the expansion of $\hat{U}(z)$ are shown in Equations (3) and (4) [10].

$$\hat{U}(z) = \frac{1}{\pi\alpha\eta} U_c(z) = -\frac{3\pi}{8} \frac{R^2}{(R+z)^5} F\left(\frac{5}{2}, \frac{5}{2}; 2; \frac{R^2}{(R+z)^2}\right) \quad (3)$$

$$\hat{U}(z) = -\frac{1}{6z^3} + \frac{1}{12Rz^2} + \ldots \quad (4)$$

Letting $R \to \infty$ and equating the two expressions for $\hat{U}(z)$ gives the final potential expression:

$$U(z) = -\frac{18\pi}{8} \frac{\alpha R^2}{(R+z)^5} F\left(\frac{5}{2}, \frac{5}{2}; 2; \frac{R^2}{(R+z)^2}\right) \quad (5)$$

Figure 1 compares the potential of a flat surface and the modified potential of a nanotube 15 nm in diameter (α = 45 K layers^3, R = 15/2 nm). The nanotube potential is seen to be

smaller even down to one atomic layer, though the deviation becomes more pronounced as the thickness increases.

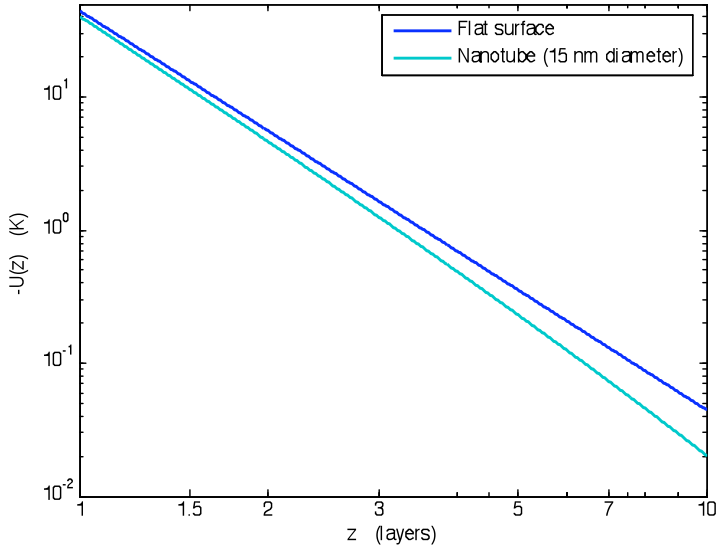

Figure 1. Van der Waals potential as a function of film thickness for a flat surface and nanotube with diameter 15 nm.

The film thickness depends on the pressure of the helium gas above the film as well as the superfluid potential. At equilibrium the chemical potential of the gas equals the potential at the superfluid surface. This relationship allows for evaluation of the film thickness d, given the gas pressure p, saturated vapor pressure p_o, bulk helium density ρ, and temperature T:

$$k_B T \ln\left(\frac{p_o}{p}\right) = -U(d) - \frac{\sigma}{\rho(R+d)} \qquad (6)$$

The curvature of the nanotube contributes a surface tension energy term shown on the right side of Equation (6) [8]. The surface tension term limits the film thickness for small values of R; for our case of 15 nm average diameter and T = 1.3 K the maximum thickness is about 6.7 atomic layers.

The speed of third sound propagation on the outer surface of a nanotube is given by Equation (7) [8]. The velocity depends on the thickness of the "dead" or nonsuperfluid thickness D_o, the density of the liquid ρ, and the bulk-liquid superfluid density ρ_s. The value of D_o can range from a fraction of one atomic layer to several atomic layers, depending on the Van der Waals force and substrate geometry.

$$c_3^2 = \frac{1}{n^2}\frac{\rho_s}{\rho}\frac{d-D_o}{d}\left(u(d) - \frac{\sigma}{\rho(R+d)^2}\right)\left(\frac{R+d}{2}\right)\left(1 - \frac{R^2}{(R+d)^2}\right), \qquad u(d) = \left.\frac{\partial U(z)}{\partial z}\right|_{z=d} \qquad (7)$$

It is important to note that Equations (1) – (6) describe superfluid adsorption and third sound propagation on one individual nanotube. In third sound experiments we adsorb the film onto a tangle of many nanotubes. The multiple scattering of the third-sound waves for such a substrate is accounted for by an index of refraction, n, in Equation (7). Capillary condensation has also been seen to affect third sound velocity on porous materials, and we speculate that similar behavior may occur at points where the nanotubes cross [11]. The

third sound speed is compared for a flat surface and for the 15 nm diameter nanotubes for different assumed values of n in Figure 2, and taking a value for D_o of 2.2 layers.

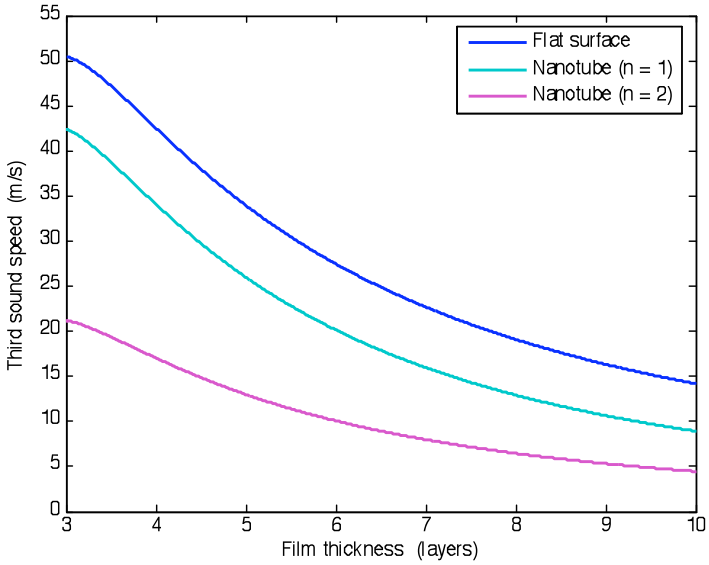

Figure 2. Third sound propagation speeds corresponding to a flat surface and nanotubes with different indices of refraction. The parameters shown correspond to those defined in

Experiment

Third sound measurement techniques were used to investigate the adsorption of ^{4}He on multiwall carbon nanotubes 10-20 nm in diameter and 10-30 microns in length. The nanotubes were sonicated for 50 minutes in ethanol and sprayed onto two Plexiglass plates using a nitrogen-pressurized sprayer. The ethanol was evaporated periodically during the spraying process, leaving a network of randomly oriented tubes attached to each surface. The resulting substrate was approximately 4 cm in length, 1 cm in width, and 15 microns thick. Before spraying, the rectangular region designated for the substrate was partitioned from the rest of the Plexiglass with tape. During spraying, some of the nanotube solution leaked outside of this region. We were able to scrape off the stray nanotubes, but it appears that the tubes were well-anchored to the surface by the spraying process. A heat source and thermal sensor were positioned in one plate at opposite ends of the substrate region to generate and detect temperature oscillations in the film. The plates were attached as shown in Figure 3, with the substrate housed in between. After assembly, the cell was placed in a standard insulated dewar and cooled to 1.3 K. A 77 K Zeolite cold trap was used to purify the helium gas metered into the cell compartment. Alumina powder was used to adsorb the bulk of the helium, thereby allowing thin films to form on the cell substrate. After each helium addition, the pressure difference between the cell compartment and helium bath was measured with a differential pressure gauge.

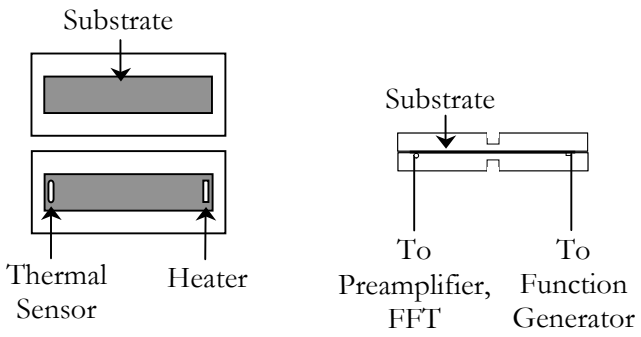

Figure 3. Top view of Plexiglass plates, indicating placement of sensor, heater, and nanotube substrates (*left*). Assembled experimental cell showing sensor and heater leads, which pass through holes in the bottom cell (*right*).

The heat source used was a band of SEM carbon paint with a low-temperature resistance of 34 K ohms. The heater output was driven by an HP 3314A Function Generator with frequency range 10– 500 Hz and 1 V maximum peak-to-peak voltage. The voltage was adjusted during the experiment in order to maximize the detected signal. A temperature-sensitive 200- Allen-Bradley resistor was used as a thermal sensor, since its resistance increases rapidly as the temperature is lowered, to about 70 K ohms at 1.3 K. Voltage changes across the resistor when it is biased with a 1 microamp current were detected with a preamplifier, and the signal was then analyzed with an FFT program in LabVIEW. Copper foil was placed between the heater and sensor to minimize the capacitive crosstalk between the two sensors. A number of standing-wave modes could be seen in the FFT curves, with the lowest few longitudinal modes being nearly harmonic. The data presented here were obtained in multiple trials using the same cell.

Results and Discussion

Preliminary third sound measurements are presented for superfluid ^{4}He films adsorbed on multiwall carbon nanotubes with average diameter 15 nm. The results come from three experimental runs. Figure 4 shows a representative sample of FFT curves taken throughout the first trial; the FFT amplitude is plotted against the propagation frequency. Relative film thickness is indicated by curve placement, the thinnest and thickest films being at the bottom and top, respectively. Distinct third sound frequency modes are visible up to approximately 600 Hz. Third sound occurs over a finite film thickness range, determined from these experiments to be between 3 and 7 layers. Frequency modes tracked throughout this region exhibit a pattern of increasing signal amplitude followed by diminishing signal strength. As the helium film thickness increases, an overall downward shift is seen in the peak frequency values. The first sign of superfluid modes, detected at 3 layers and designated by a black arrow in Figure 4, diminishes significantly in the next curve, and then reappears in the subsequent curves at higher thickness. This apparent re-entrant behavior in the superfluidity prompted further investigation into the onset region.

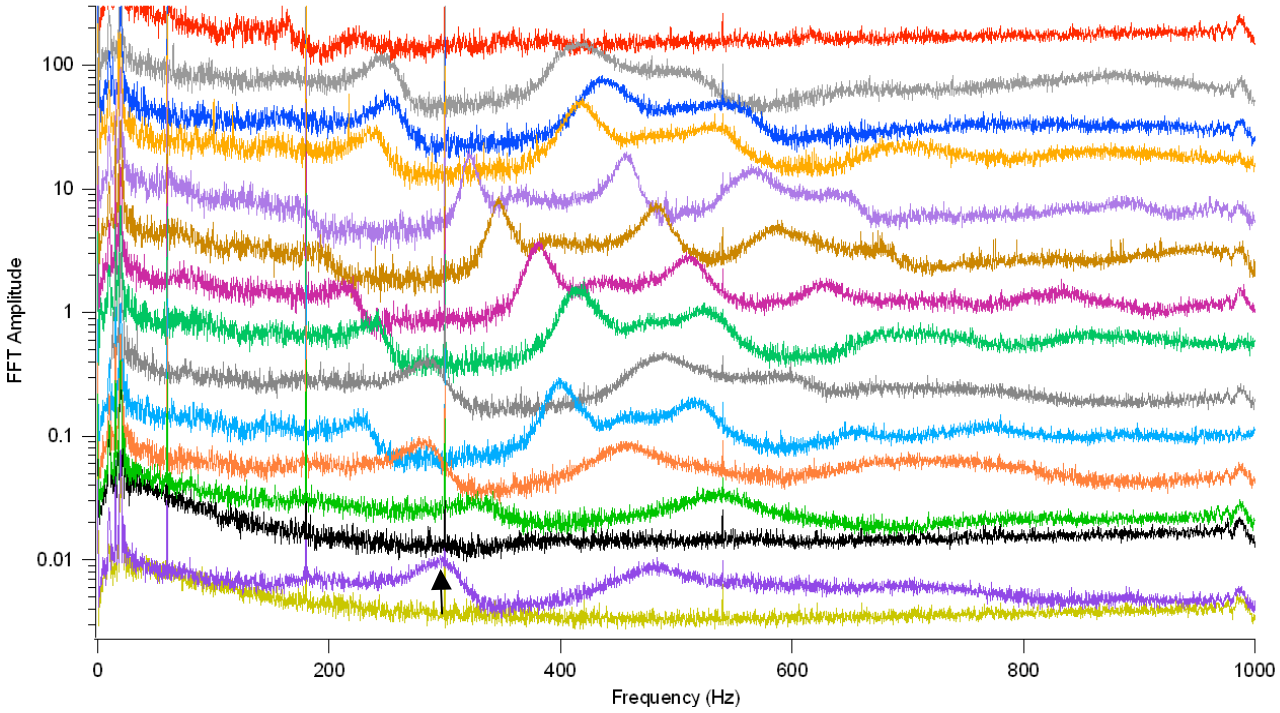

Figure 4. Sample of FFT amplitude versus frequency curves taken from the first run. The black arrow indicates the first onset signal.

In the second run, the film was built up slowly by adding smaller increments of helium to better follow the signal progression near the onset point. The results are shown in Figure 5(a), starting with the first observed signal at 3.12 layers. The data taken before this point has been omitted due to excessive noise. Though the signal is clearly much weaker than that detected in the first experiment, the signal again diminishes before re-entering in the topmost curves. The film was built up slower still in the third run [see Figure 5(b)], with the results closely resembling the second run. The two later runs show only one resonant mode around 300 Hz. The signal was found to be strongest with a 1 V heater voltage, though it was still visible at .75 V. A 2 V drive appeared to be too high to create detectable propagation in the thinner films.

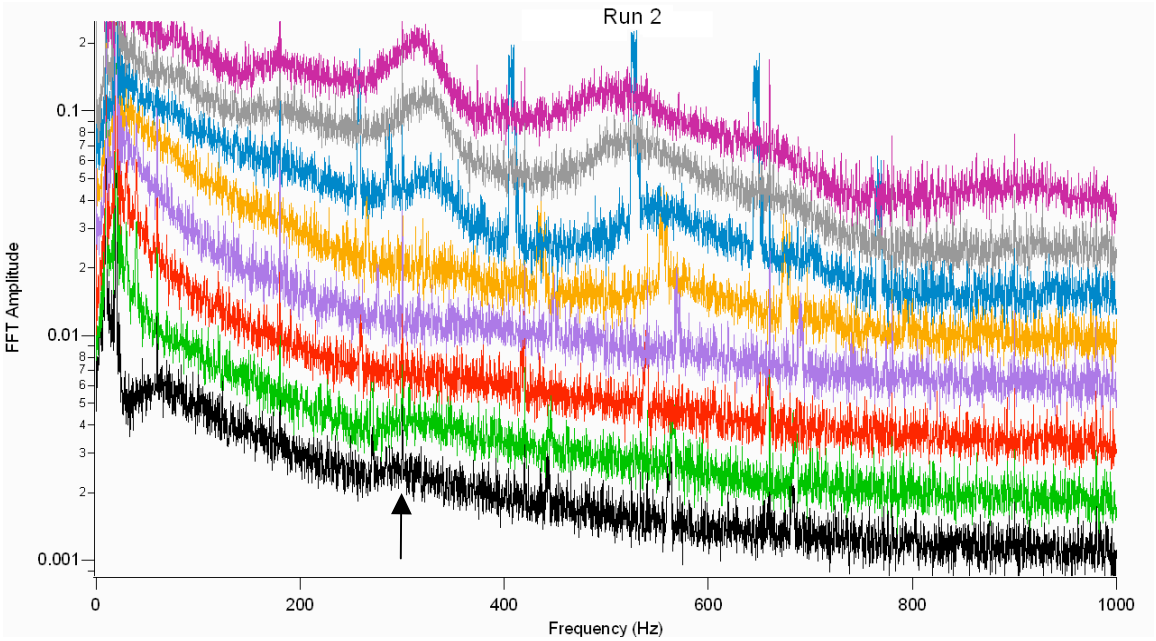

(a)

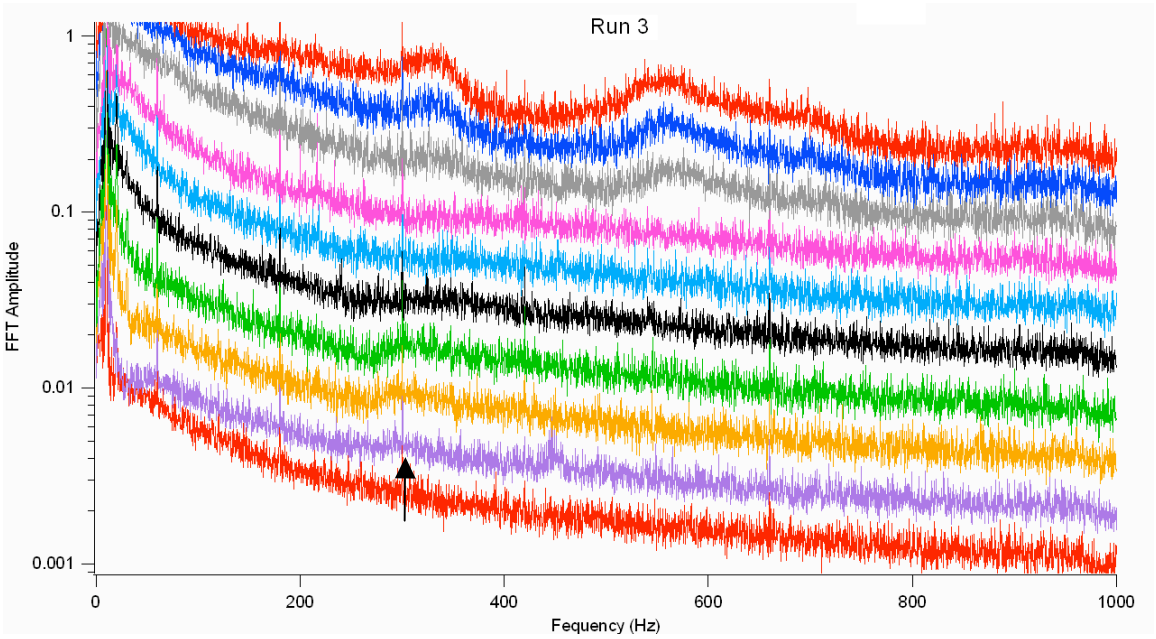

(b)

Figure 5. Superfluid onset and subsequent decrease in superfluid signal from (a) run two and (b) run three. Black arrows indicate the initial onset signal around 300 Hz.

Figure 6(a) shows the experimental third sound speed from Run 2. The theoretical speed is also plotted with the parameter K = .07, where K is taken to be $\frac{1}{n^2}\frac{\rho_b}{\rho}$, to best fit the data. Rearrangement of the film due to the disturbance induced by helium transfers may account for the overlap observed around 4 and 5 atomic layers. The theoretical and experimental speeds from Run 3, shown in Figure 6(b), seem to match the results from Run 2; the best fit parameter used in Figure 6(b) was again K = .07. Both graphs exhibit an overall pattern of decreasing speed with increasing film thickness as expected. However, both graphs also show the re-entrant superfluidity corresponding to the first signals detected before the main onset at thicker films. In addition, there is also a break in the downward trend observed in Figure 6(b) between 5.5 and 6.5 layers. A similar effect may occur in Figure 6(a), though more data are needed to verify if this is the case.

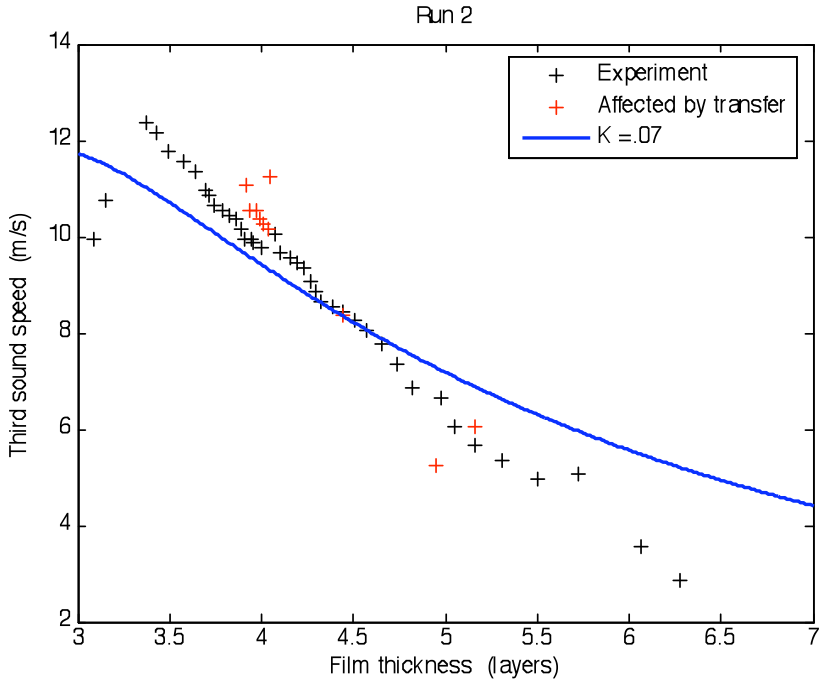

(a)

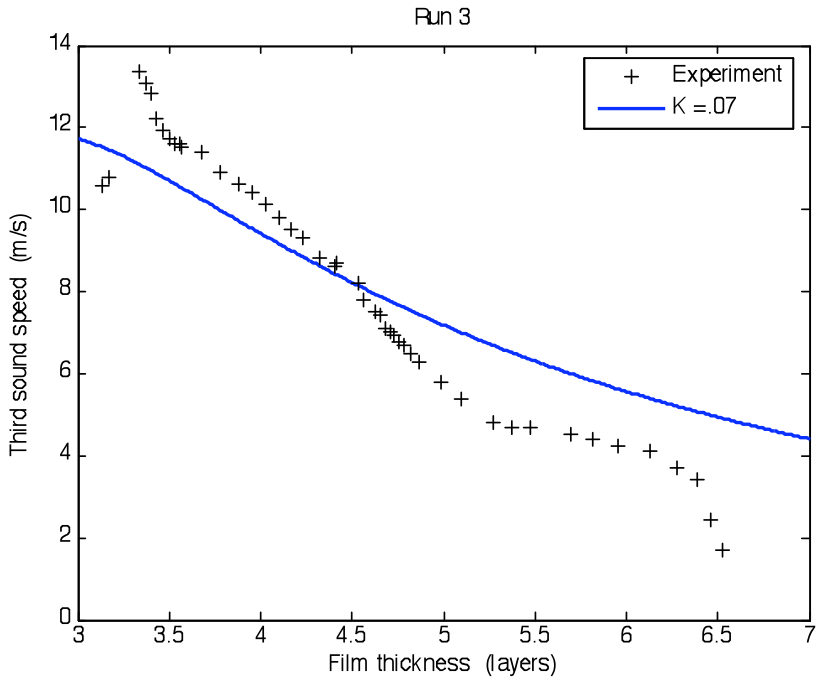

(b)

Figure 6. Experimental and theoretical third sound velocities from (a) run two and (b) run three. The theoretical curves are fit to the data using K = .07, where K is defined in the text.

The observed re-entrant behavior in the superfluidity between 3 and 3.5 atomic layers is an unusual and interesting result. This pattern has been detected in each of the experiments, though the magnitude of the signal has not been consistent. It is unclear why the signal appeared so exaggerated in the first experiment. Though the film thickness was built up in smaller increments with each successive experiment to capture the onset progression, the initial signal had a much smaller amplitude in these later runs.

Previous studies report a temporary loss of superfluidity on flat sheets of graphite at 2 atomic layers [12,13]. Crowell and Reppy attribute the destruction and re-entrance to solidification of the helium as it builds up in layers [14]. A similar effect of quasi-solidification may occur on the surface of the graphite nanotubes, causing the drop in superfluid signal above 3 layers. The results we have seen were obtained by running the experiment at 1.3 K, while the results on flat graphite were only seen at temperatures well below 1 K. Further work is needed to better understand the results presented here; in particular it would be worthwhile to perform third sound measurements using multiwall nanotubes at lower temperatures.

Acknowledgements

This research was supported by the National Science Foundation and the UCLA Department of Physics and Astronomy. I thank Gary Williams for his support and guidance, as well as Hossie Fard, Emin Menachekanian, and Guanyu Zhu for their assistance

with the project. I also thank Françoise Quéval for her efforts in organizing the REU program.

References

[1] G.A. Williams, Endeavour **16**, 102 (1992).
[2] D.J. Bishop, J.E. Berthold, J.M. Parpia, and J.D. Reppy, Phys. Rev. B **24**, 5047 (1981).
[3] V. Kotsubo and G.A. Williams, Phys. Rev. B **33**, 6106 (1986).
[4] G.A. Williams, J. Low Temp. Phys. **110**, 567 (1998).
[5] J. Machta and R.A. Guyer, J. Low Temp. Phys. **74**, 231 (1989).
[6] H. Chu and G.A. Williams, J. Low Temp. Phys. **138**, 343 (2005).
[7] S. Iijima, Physica B **323**, 1 (2002).
[8] G.A. Williams, S. Vo, H. Fard, and A. Kogar, in *25th International Conference on Low Temperature Physics*, Amsterdam, Netherlands, 2008.
[9] G.A. Williams, in *Encyclopedia of Acoustics*, edited by M.J. Crocker (John Wiley & Sons, Inc., Hoboken, NJ, 1997) p. 673.
[10] V.A. Kirsch, *Adv. Colloid Interface Sci.* **104**, 311 (2003).
[11] R. Rosenbaum, G.A. Williams, D. Heckerman, J. Marcus, D. Scholler, J. Maynard, I. Rudnick, J. Low Temp. Phys. **37**, 663 (1979).
[12] P.A. Crowell and J.D. Reppy, Phys. Rev. Lett. **70**, 3291 (1993).
[13] J.D. Maynard and M.H.W. Chan, Physica 109 & 110B, 2090 (1982).
[14] P.A. Crowell and J.D. Reppy, Phys. Rev. B **53**, 2701 (1996).